Huu Duc Vo
Department of Mechanical Engineering,
École Polytechnique de Montréal,
2900 boul. Edouard-Montpetit,
2500 ch. de Polytechnique,
Montreal, Quebec, H3T 1J4, Canada
e-mail: huu-duc.vo@polymtl.ca

Choon S. Tan
e-mail: choon@mit.edu

Edward M. Greitzer
e-mail: greitzer@mit.edu

Department of Aeronautics and Astronautics,
Massachusetts Institute of Technology,
77 Massachusetts Avenue,
Cambridge, MA 02139

Criteria for Spike Initiated Rotating Stall

A computational study to define the phenomena that lead to the onset of short length-scale (spike) rotating stall disturbances has been carried out. Based on unsteady simulations, we hypothesize there are two conditions necessary for the formation of spike disturbances, both of which are linked to the tip clearance flow. One is that the interface between the tip clearance and oncoming flows becomes parallel to the leading-edge plane. The second is the initiation of backflow, stemming from the fluid in adjacent passages, at the trailing-edge plane. The two criteria also imply a circumferential length scale for spike disturbances. The hypothesis and scenario developed are consistent with numerical simulations and experimental observations of axial compressor stall inception. A comparison of calculations for multiple blades with those for single passages also allows statements to be made about the utility of single passage computations as a descriptor of compressor stall. [DOI: 10.1115/1.2750674]

Keywords: compressor instability, rotating stall, spike stall inception, tip clearance flow

Introduction

There are two well-established routes to rotating stall, referred to as long length-scale or "modal" inception and short length-scale or "spike" inception, with the two routes distinguished by the type of initial perturbation in pressure/velocity. The former is characterized by the evolution, in tens of rotor revolutions, of a small amplitude disturbance with wavelength on the order of the annulus circumference, into a fully developed stall cell with approximately the same propagation speed. This type of stall inception is well described by so-called actuator disk models, which consider the overall effects of the blading, in essence smearing out the details of the flow on the blade scale. It has been shown both analytically [1,2] and experimentally [3] to occur at conditions at, or slightly beyond, the peak of the stagnation-to-static pressure rise of the compressor.

Many compressors, however, exhibit a short length-scale, or spike, stall inception. This phenomenon, which is less understood, was first described by Day [4]. It is characterized by the appearance of a disturbance (or "spike") two to three blade pitches in width at the rotor tip. The spike rotates at about 70% of the rotor speed and can grow into a two-dimensional stall cell more rapidly than in modal inception, within roughly three rotor revolutions. During this process, in contrast to modal stall inception, the propagation speed of the disturbance typically drops to below 50% of rotor speed. Also in contrast to modal stall, spike stall inception is observed to occur at flows where the stagnation-to-static pressure rise characteristic has a negative slope.

Unlike long length-scale stall inception, where the small amplitude of the modal disturbance lends itself to linear analysis, the velocity defect associated with the spike disturbance is comparable to the mean velocity through the compressor, and a nonlinear approach is required. Features of the evolution of an *input* spike disturbance into fully developed rotating stall have been captured using a nonlinear simulation that employed a three-dimensional distribution of body forces (again, smearing out the effects of discrete passages) by Gong et al. [5]. However, the more important process from the point of view of defining the conditions under which the process starts, in other words *the origin of the spike*, has not been resolved. These conditions are described in the present paper. They differ fundamentally from existing stall analyses in that the disturbance nature and scale is such that the structure of the flow within the passages, not just the integrated effects of the blade rows, must be addressed.

The experimental measurements of Day [4] show that the spikes are not only circumferentially localized, but are confined to the tip region of a rotor, leading to the possible association of their origin with the tip clearance flow. As such, the basic issue addressed in this paper is the causal link between tip clearance flow and spike stall inception, i.e., what is the mechanism (and the conditions) by which tip clearance flow leads to the formation of short length-scale rotating stall disturbances?

The paper is organized as follows. Rotor passage flow features common to compressors exhibiting spike stall inception are first identified. This allows focus on a particular rotor geometry while supporting the generic nature of the study. Time-accurate single blade passage computations are then used to define the criteria that set the single blade passage solution limit—referred to here as the *flow solution limit*—which is the lowest flow coefficient for which a steady solution exists. This is followed by a six blade passage flow simulation to clarify the link between tip clearance flow and spike disturbances and the utility of single blade passage solution limit as guideline for predicting compressor stall inception. The findings are then used to explain observed spike stall inception behavior.

Rotor Flow Features of Spike Stall

Single blade passage computations [6] on different compressor rotors that are known to exhibit spike stall inception indicate that the flow solution limit occurs when the interface between the incoming flow and tip clearance flow lines up with the rotor leading edge plane. Figure 1 shows the trajectory of the interface between the incoming and tip clearance flows [7]. The position of this interface results from a balance between the momentum of the incoming flow and that of the tip clearance flow. As the flow coefficient decreases, the axial momentum of the incoming flow reduces and the blade loading, which drives tip clearance flow and thus increases the momentum of the flow through the clearance [8], rises. The result is a movement of the interface toward the rotor leading edge plane, as observed from rotor casing oil flow pictures by Koch [9] and Saathoff and Stark [10]. The latter examined a low-speed compressor near the point of spike stall in-

Contributed by the International Gas Turbine Institute of ASME for publication in the JOURNAL OF TURBOMACHINERY. Manuscript received June 23, 2006; final manuscript received June 30, 2006; published on January 30, 2008. Review conducted by David Wisler. Paper presented at the ASME Turbo Expo 2005: Land, Sea and Air (GT2005), June 6–9, 2005, Reno, NV.

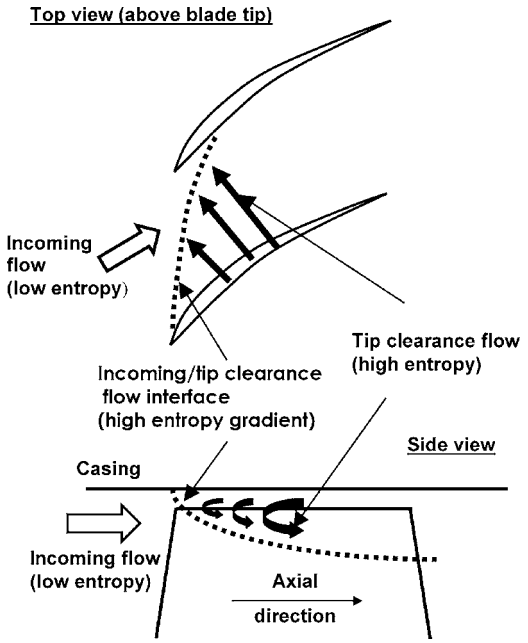

Fig. 1 Sketch of incoming/tip clearance flow interface

ception and found that the stall limit occurred when the interface was aligned with the leading edge. This will be seen to be a feature of the computations to be described.

In the computations, entropy/unit mass is used to track the interface. The tip clearance flow mixes after leaving the clearance, has higher entropy than the incoming flow, and the interface is a region of high entropy gradient. Contours of computed entropy/unit mass on the rotor blade tip radial plane at the flow solution limit, based on steady RANS computations, are shown in Figs. 2 and 3 for the low Mach number ($M_{tip} \approx 0.2$) E^3 rotor B and for the transonic rotor from NASA stage 35, respectively. Both of these are known to exhibit spike stall inception, the latter when subjected to inlet radial distortion [11,12]. The computations show that when the solution limit is reached the incoming/tip clearance flow interface is aligned with the rotor leading-edge plane at the blade tip. We cite these results to indicate that even with the large differences in design conditions a similar set of phenomena occur at the flow solution limit. The E^3 rotor B has the additional advantage of not exhibiting flow separation on the blade, allowing clearer isolation of the role of tip clearance flow on the flow solution limit. We thus focus on this rotor as a vehicle for establishing the context of the flow solution limit in relation to the onset of spike disturbances and in defining the role of tip clearance flow in the latter process.

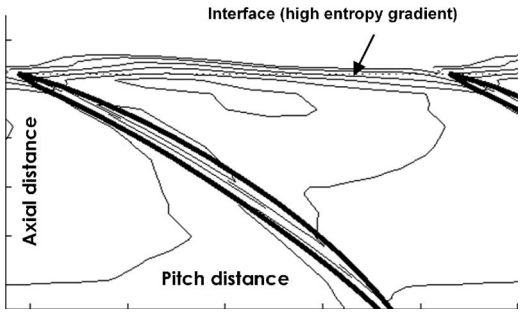

Fig. 2 Contours of entropy/unit mass at E^3 rotor blade tip at the flow solution limit

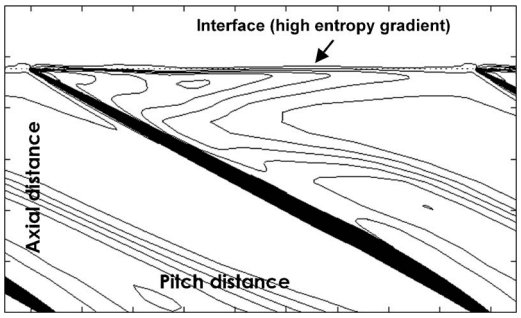

Fig. 3 Contours of entropy/unit mass at rotor 35 blade tip at flow solution limit/stall point

Features of Transients Beyond the Flow Solution Limit

Time-accurate single blade passage computations using UNSTREST [13], as described in the Appendix, were used to assess the behavior of the tip clearance flow beyond the flow solution limit and to identify the threshold flow events leading to spike stall inception. This involved incrementally increasing the exit tip pressure until the occurrence of a rapid transient, including a large drop in mass flow beyond the flow solution limit. The computed total-to-static pressure rise versus flow coefficient, seen in Fig. 4, shows both the steady-state flow regime (points 1–4) and the transient regime (points 5–8). The tip clearance was 1.8% chord. The corresponding variations of total blockage and the individual contributions (tip clearance blockage and passage-blade/hub-boundary layer blockage) [7] are also given. The flow solution limit (point 4) coincides with a rapid growth in blockage. This growth comes only from the tip blockage; blockage from blade and hub boundary layers does not grow as the flow coefficient drops below the flow solution limit.

One feature of the transient is the spillage of tip clearance flow to the adjacent blade passage ahead of the rotor leading edge and below (inboard of) the blade tip radius. This is sketched in Fig. 5, which shows the path of tip clearance flow fluid spilling into the next blade passage, a scenario suggested by Cumpsty [14]. Figure 6 shows the mass flow through the blade clearance (i.e., over the blade tip) and the mass flow spilling ahead of the blade leading edge below the blade tip. The operating points correspond to those in Fig. 4. The amount of spilled fluid increases while the amount flowing over the blade tip decreases, as the flow coefficient decreases below point 3. There is no leading-edge spillage below the blade tip at point 3, at a flow coefficient just above the flow

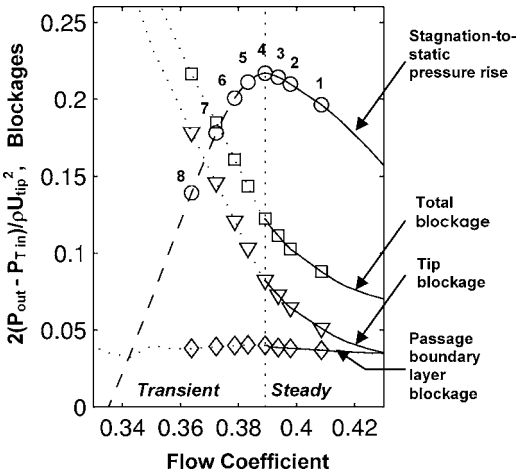

Fig. 4 Passage pressure rise and blockage as a function of flow coefficient for E^3 rotor B; 1.8% chord tip clearance

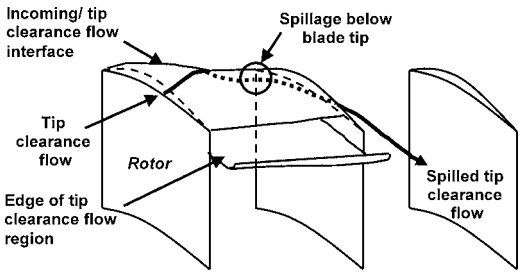

Fig. 5 Leading-edge tip clearance flow spillage below blade tip

solution limit (point 4). The onset of flow spillage below the blade tip means that the incoming/tip clearance flow interface crosses the blade leading edge. This is the common flow feature associated with compressors exhibiting spike stall inception identified in the previous section.

Figure 7 illustrates a second feature seen at flow coefficients below the flow solution limit. Fluid originating from the tip clearance moves (from an adjacent blade passage) into the blade passage *at the trailing edge*. The trajectory of this fluid is such that there is impingement on the pressure surface. This reversal of the tip clearance fluid from the adjacent blade passage (essentially an end-wall separation with a circumferential relative velocity component) will be referred to as "tip clearance backflow." The spanwise distribution of pitch-averaged mass flow (nondimensionalized by inlet stagnation density and blade tip speed) in Fig. 8 shows the onset of tip clearance backflow below the blade tip at the flow solution limit. The operating point numbers again correspond to those in Fig. 4. For steady-state solutions (points 1–3), Fig. 8 shows downstream (positive) mass flow below the blade tip. At the flow solution limit (point 4), the mass flow reaches zero at the blade tip. It then becomes negative for transient points at lower flow coefficients (points 5–8), signifying backflow below the blade tip.

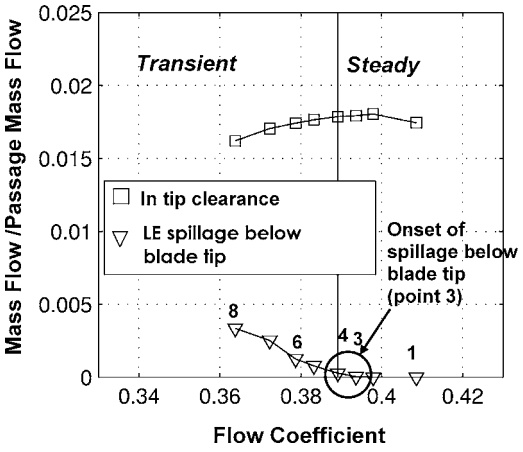

Fig. 6 Mass flow through tip clearance and mass flow spilled ahead of leading edge below blade tip

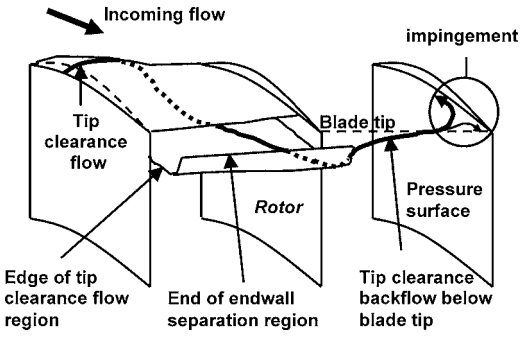

Fig. 7 Reversal ("backflow") of tip clearance fluid below the blade tip

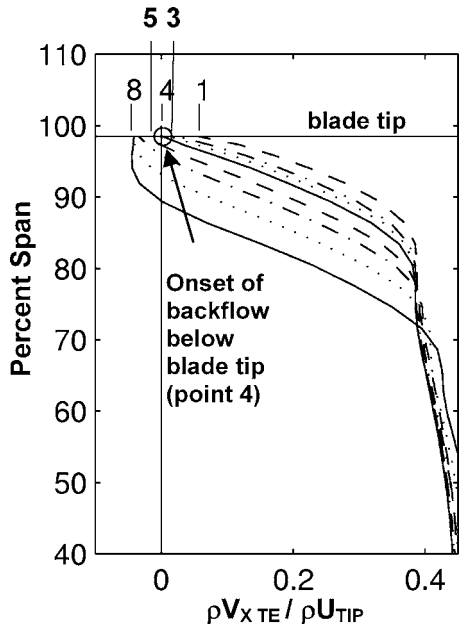

Fig. 8 Spanwise distribution of pitch-averaged mass flow at passage exit plane (1.8% chord tip clearance)

We can now consider how the above threshold flow events set the flow solution limit and contribute to the observed blockage growth. Figure 9 illustrates the connection between the impingement (sketched in Fig. 7) and the generation of higher blockage. The figure shows relative velocity vectors (Figs. 9(*a*) and 9(*c*)) and static pressure contours (Figs. 9(*b*) and 9(*d*)) at the blade tip radius, at two times corresponding to points 6 and 8 in Fig. 4. Features of interest are marked with circles. There is no pitch-average backflow below the blade tip at the trailing edge at the flow solution limit, but if the back pressure is increased, backflow occurs. Impingement of this backflow on the pressure surface increases the local pressure gradient at the rear of the blade passage, as shown by the more closely-spaced static pressure contours in Fig. 9(*d*) compared to Fig. 9(*b*). This drives the backflow upstream (Fig. 9(*c*) compared to Fig. 9(*a*)). The upstream movement of this fluid in turn leads to a further enhancement in backflow and additional local pressure rise from impingement, thus providing positive feedback and a conduit for further tip blockage increase.

We can also connect the tip clearance backflow to the observed increase in tip blockage beyond the flow solution limit. Figure 10 shows the variation with flow coefficient of the tip region blockage, evaluated at the trailing-edge plane, for the conditions of Fig. 4. The contributions from backflow (regions of negative axial velocity) and from local tip clearance fluid (tip blockage–backflow blockage) to the tip region blockage are also shown separately. For the transient flow regime (between points 4 and 8), the rate of increase in blockage associated with backflow accounts for most of the rate of increase in tip blockage.

Figure 11 illustrates the role of leading-edge spillage in setting the flow solution limit. The upper sketch (Fig. 11(*a*) depicts the tip clearance flow trajectory for a situation in which spillage has not occurred, and the lower sketch (Fig. 11(*b*)) the trajectory when there is leading-edge spillage. With the incoming/tip clearance flow interface inside the passage (no leading-edge spillage, as in Fig. 11(*a*)), the tip clearance fluid, as well as any backflow, either

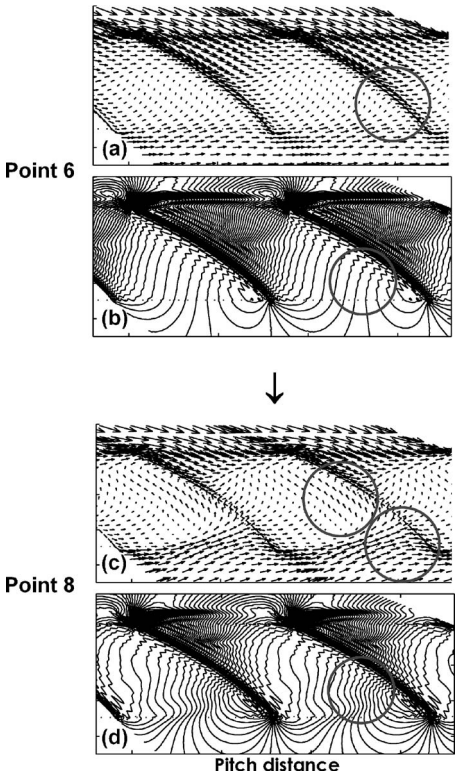

Fig. 9 Relative flow vectors and static pressure contour at rotor tip plane during transient beyond equilibrium solution limit. Figs. 9(*a*) and 9(*b*) correspond to point 6, and Figs. 9(*c*) and 9(*d*) to point 8, of Figs. 4, 6, and 8.

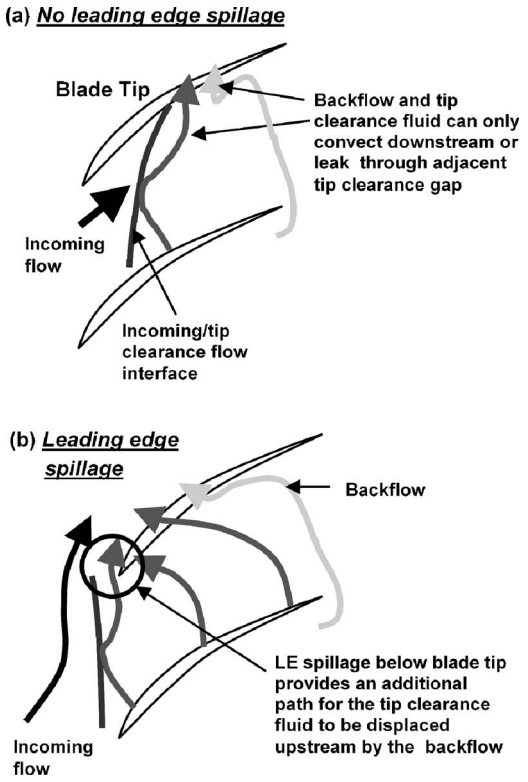

Fig. 11 Role of leading-edge spillage on upstream propagation of backflow

convects downstream or leaks through the adjacent tip clearance. However, leading-edge spillage below the blade tip (as in Fig. 11(*b*)) means that the tip clearance fluid has an additional path by which it can move upstream, especially when displaced by the backflow.

Although the two threshold flow events may start at different flow coefficients, the hypothesis of this paper is that both must be present (i.e., both criteria must be satisfied) for the flow solution limit to be reached. The flow solution limit will occur at the lower of the two flow coefficients at which the threshold flow events occur.

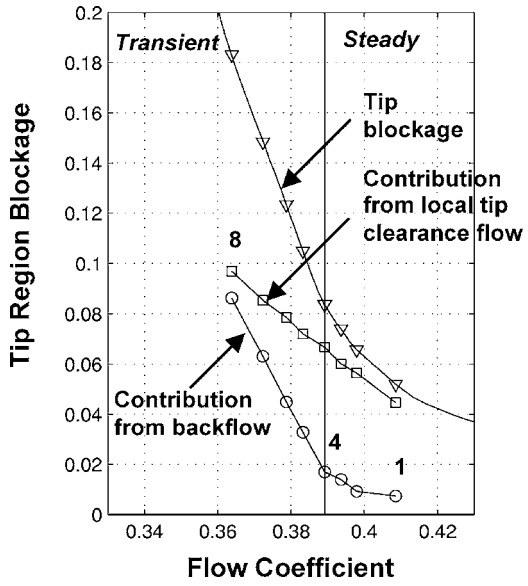

Fig. 10 Contribution of tip clearance backflow to overall tip region blockage

As an illustration of the above, tip clearance backflow can start at a higher flow coefficient than leading-edge spillage, but the flow solution limit will only occur when the latter appears. This is demonstrated by E^3 rotor B computations carried out at 3.0% chord tip clearance, where there is appreciable separation between the conditions for the occurrence of the two events and where the backflow occurs at a much higher flow coefficient than spillage. Figure 12 shows a time-averaged[1] pressure rise coefficient and pitch-averaged mass flow and spillage mass flow distributions. The symbols are the same as those in Figs. 4, 8, and 6, respectively.

Figure 12(*b*) shows the spanwise distribution of pitchwise average mass flow at the trailing edge. Backflow below the blade tip is seen at flow coefficients as high as point 1. However, the flow solution limit does not occur until the onset of leading edge spillage below the blade tip at point 4 (see Fig. 12(*c*)), where both conditions are satisfied.

In the converse situation, leading edge spillage can occur at a higher flow coefficient than the backflow, but again, the flow solution limit is reached only when backflow below the blade tip occurs. This situation is shown in Figs. 6 and 8 for the 1.8% chord tip clearance case. From Fig. 6, leading-edge spillage is seen to start at point 3. However, the flow solution limit for this case occurs at point 4, at the onset of trailing edge backflow (Fig. 8).

The link between the single passage flow solution limit and the tip clearance flow can thus be summarized as follows:

- The flow solution limit is characterized by the onset of rapid

[1]For large tip clearance sizes, as is the case here, steady oscillations in the tip clearance flow were found to occur near the flow solution limit. The values reported are thus time averaged. Similar oscillations were observed by Mailach et al. [15] and Marz et al. [16]

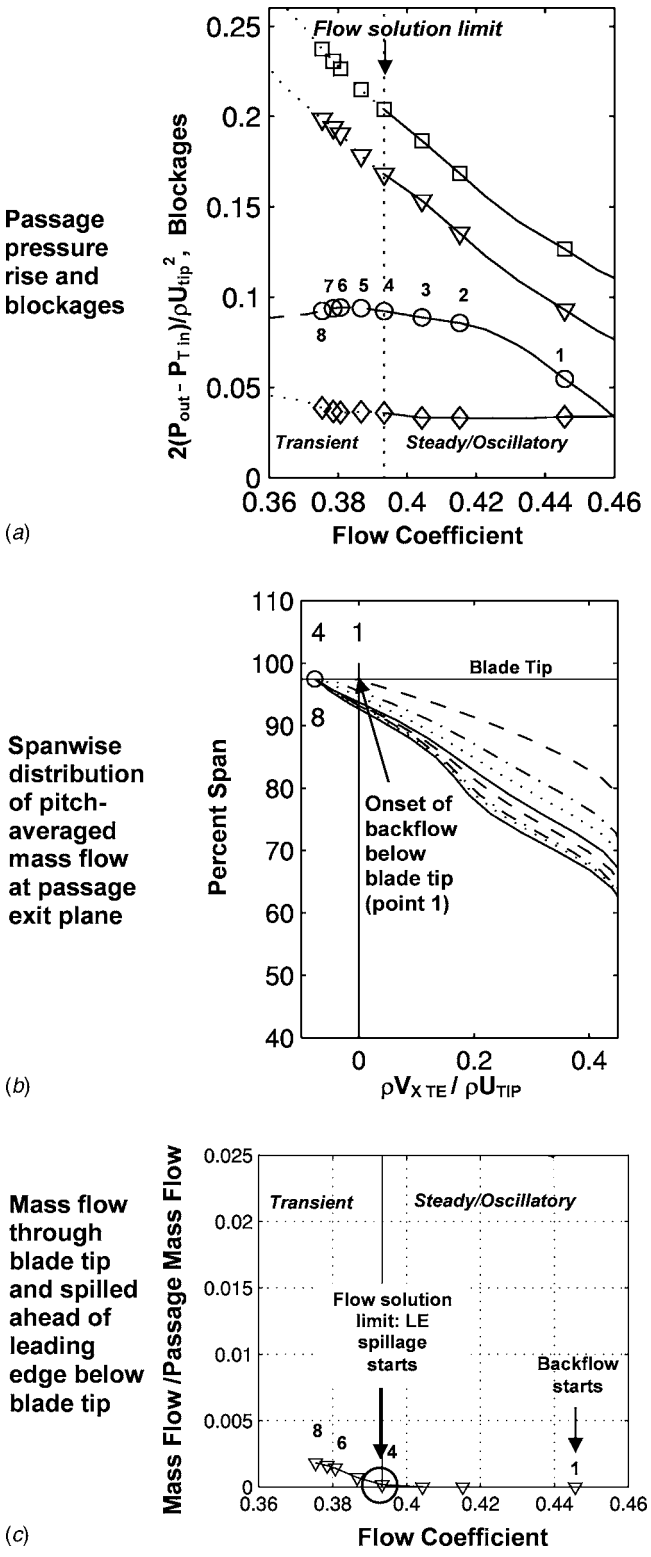

Fig. 12 Evaluation of passage flow solution limit criteria for 3.0% chord tip clearance: (*a*) passage pressure rise and blockages, (*b*) spanwise distribution of pitch-averaged mass flow at passage exit plane, and (*c*) mass flow through blade tip and spilled ahead of leading edge below blade tip

transient growth of the passage tip blockage until the tip blockage grows to the hub.

- The onset of the tip blockage growth is marked by two threshold flow events/criteria, which can start at different flow coefficients but must both be present:
  1. Backflow of tip clearance fluid (zero pitch-averaged mass flow across the pitch) from adjacent blade passages at the trailing edge plane below the blade tip
  2. Spillage of tip clearance fluid ahead of the blade leading edge below the blade tip into the next passage

In the next section, we connect this description of the blade passage flow solution limit with the formation of spike disturbances. We view four factors as underpinning this connection. First, is that the phenomena described occur in the tip region, where spike disturbances have been experimentally detected. Second, is that the spillage of tip clearance fluid to the adjacent blade passage ahead of the rotor leading edge is consistent with the generic flow features associated with spike stall inception, where the incoming/tip clearance flow interface lines up with the rotor leading-edge plane. Third, we have observed the impingement pattern of trailing-edge backflow in the stall computations by Hah et al. [17] on another low-speed rotor. Finally, the required presence of both threshold flow events for stall inception is observed in the study of rotating instabilities by Marz et al. [16]. Trailing-edge backflow can be seen in their multiple blade passage computations in the stable flow range, but they state that stall does not occur until the tip clearance flow leaks across the blade leading edge.

Link to Stall Inception

Multiple blade passage unsteady computations have been carried out to provide detailed comparison of the proposed criteria for single blade passage flow solution limit with the inception of rotating stall. In addition, the scenario for spike formation has been assessed against known experimental observations on stall inception. Both of these comparisons bear out both the scenario and the hypothesized criteria.

Six blade passages were used to simulate the formation of spike stall disturbances. While six passages are not ideal, two reasons can be put forward as an argument that the calculation demonstrates the central features of the spike waveform. First, the slope of the total-to-static pressure rise characteristics at the flow solution limit is negative and, thus, the only known route to rotating stall is via spike formation [3]. Second, spike disturbances have been experimentally measured to have a circumferential extent of two to three blade passages [4,11,18,19].

As described in the Appendix, the computational code, mesh, and procedure were the same as for the single blade passage computations. The single blade passage flow field corresponding to the flow solution limit was used for the initial condition. The equivalence between single and multiple blade passage flow solution limits is evidenced by the fact that, in the absence of any introduced asymmetry in the flow field, all blade passages stall simultaneously with the same transient beyond the flow solution limit as the single blade passage computation. To provide the circumferential nonuniformity associated with rotating stall, therefore, a small amplitude sinusoidal disturbance in stagnation pressure (velocity nonuniformity corresponding to ~1% of wheel speed and wavelength of six passages) was introduced upstream. The applied disturbance only existed during the first ten blade-pitch convection times, well before any spike disturbance formation and it extended over the full span. These initial disturbances, which favor modal stall inception rather than spikes at the tip, were chosen to ensure that the spikes would grow "naturally," rather than being forced by an initial disturbance.

Figure 13 shows results for the multiple blade passage stall simulation. There are five plots in Fig. 13. The uppermost one gives the time history of the mass flow during the stall transient. The lower four show the axial velocity deviation from the passage-averaged value, normalized by blade tip velocity, at the

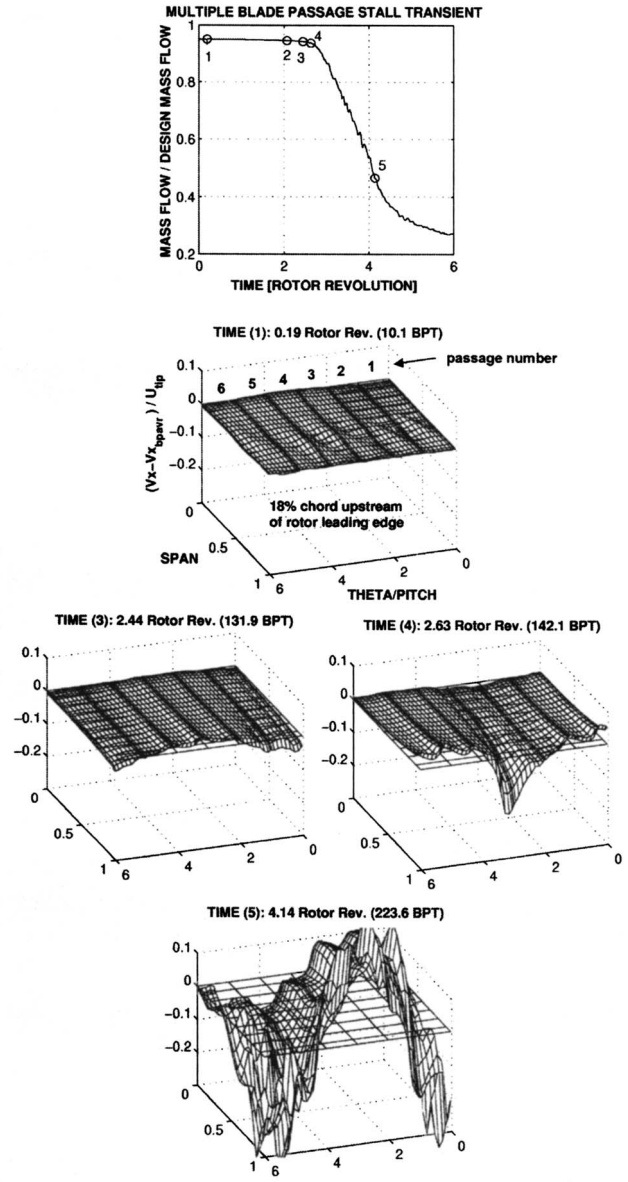

Fig. 13 Stall transient for multiple (six) blade passage configuration

different times marked in the mass flow time history. The three axes on the figure are axial velocity, span (going from 0 at the hub to 1.0 at the tip) and circumferential coordinate theta measured in blade pitches. The axial position of the plots is 18% chord upstream of the rotor leading edge, representative of hot-wire locations used in published measurements of spike disturbances (e.g., [4]).

At time instant (1), when the initially imposed disturbance is removed, no visible velocity defect at the blade tip is seen, implying the introduced flow asymmetry has not biased the results in favor of spikes. A short length-scale disturbance (in the form of an axial velocity deviation near the casing that is more pronounced at the crest) appears at time (3). At time (4), a velocity defect near the casing, which is localized over roughly two blade pitches becomes visible, accompanied by the start of a rapid drop in the mass flow. The disturbance grows rapidly in amplitude and also becomes more two-dimensional, as seen at time (5).

On the axial velocity deviation plots in Fig. 13, the direction of blade motion is from left to right along the *theta/pitch* axis. With respect to the blades the velocity defect (short length-scale disturbance) moves in the reverse direction because its speed is less than blade speed in the absolute frame of reference. The speed of the short length-scale disturbance can be estimated from the position of the maximum velocity deficit at different times, as in the experiments. The maximum velocity defect has moved by about three blade pitches between time steps (3) and (4), which are ten blade passing times (BPT) apart. The speed of the disturbance is thus ~70% of the rotor speed. The time scale of the growth to fully developed stall in the computations is essentially the time needed from inception (say time between (2) and (3)) until the disturbance extends across the entire span (roughly a revolution after time (5)), overall about three rotor revolutions.

Table 1 Comparison of measured [5] and computed spike disturbance for E^3 rotor B

Characteristics	Experiment	Computation
Circumferential extent	~2–3 blade pitch	~2–3 blade pitch
Radial extent	concentrated in tip region	last 10–20% span
Rotating speed	70–73% of rotor speed	~70% of rotor speed
Growth time to full stall cell	~3 rotor revolutions	~3 rotor revolutions

Table 1 compares the computed short length-scale disturbance to hot-wire measurements of spike disturbance in front of the E^3 rotor B [11] as summarized by Gong et al. [5]. The features of the disturbance obtained from the computations compares well to the measured features.

We also need to assess whether the criteria and scenario for spike disturbance formation are consistent with those for the single blade passage flow solution limit. To do this we examine: (i) tip clearance backflow at the trailing edge and (ii) leading edge tip clearance fluid spillage, for the blade passage behind the spike disturbance. Figure 14 displays the relative flow vectors at the blade tip radius at time (4). Figure 15 presents the relative flow vectors for the single blade passage calculation in the transient regime (beyond point 8 in Fig. 4) at a flow coefficient (0.343) near that (0.346) of passage 3 in Fig. 14. The two threshold events (flow spillage at leading edge and backflow at trailing edge) proposed as necessary for spike disturbance formation can be seen in both the multiple and single blade passage solutions.

Figure 16 shows the spanwise distribution of pitch-averaged mass flow and leading-edge tip clearance fluid spillage below the blade tip, for each blade passage at time (4). At this time, the velocity defect is in front of blade passages 3 and 4 and is moving toward blade passage 5. Figure 16 can be compared to Figs. 8 and 6 for the single blade calculations. In Figs. 14 and 16(*a*), passages 3 and 4 show trailing-edge backflow and impingement below the blade tip due to tip clearance fluid from adjacent blade passages. The other blade passages do not exhibit any trailing-edge backflow below the blade tip. Figures 14 and 16(*b*) also show leading-edge spillage of tip clearance fluid below the blade tip from blade passage (3) into passage (4). These two flow events are similar to those observed in the single blade passage flow transient past the flow solution limit.

Our inference from the multiple passage stall simulation is thus that the criteria, which set the single blade passage flow solution limit, also describe the conditions for the formation of spike stall disturbances. The flow solution limit is therefore viewed as a sufficient condition for spike formation although it is not a necessary one. A disturbance of sufficient amplitude introduced at a higher mass flow could trigger spike formation. However, even in this case, we expect the proposed spike formation scenario in terms of tip clearance backflow and spillage to apply.

The multiple blade passage stall simulation also provides in-

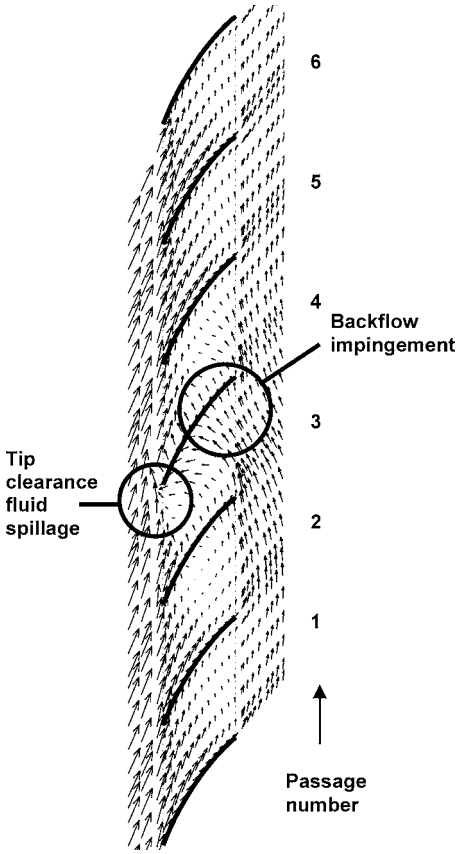

Fig. 14 Relative flow vectors at blade tip at time 4 of stall transient in Fig. 13

sight into the length scale of the spikes. The two criteria that set the single blade passage flow solution limit have a minimum of two passages as their circumferential extent and, at least as observed in all the calculations we have done, an extent of three passages for the maximum. In Fig. 14, all the leading-edge spillage fluid from the passage (3) flows into passage (4) such that the disturbance is most pronounced for these two passages. The backflow tip clearance fluid may come mainly from passage (2), but also from one or two passages beyond. Although quantitative scaling is yet to be done, the above extent relates well to the observed circumferential extent of the spikes.

Although not shown in this paper, we note that the computational results and criteria for spike formation are also in accord with the following experimental observations:

1. The blade loading at which both the backflow and spillage criteria occur corresponds to the critical tip incidence that Camp and Day [3] found for spike formation.
2. The best place to detect the spike disturbance on the E^3 compressor was at the trailing edge of the first rotor near the casing [20]. Details relating to items 1 and 2 are given by Vo [6].
3. Recent experiments by Deppe et al. [21] confirm the presence of both leading-edge spillage and trailing-edge backflow during spike formation on three different low-speed single-stage compressors.

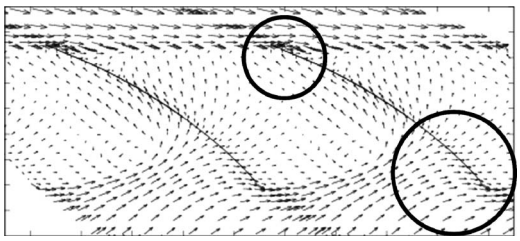

Fig. 15 Relative flow vectors at blade tip in single blade passage computation at a flow coefficient near that of passage 3 in Fig. 14

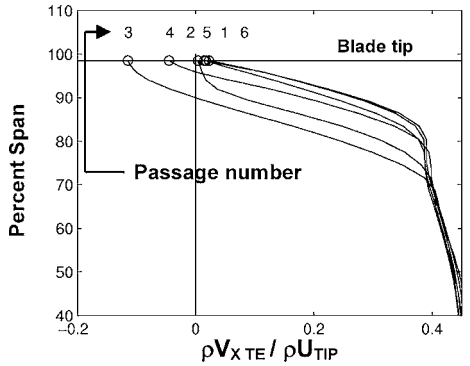

(*a*) **Spanwise distribution of pitch-averaged mass flow at passage exit plane**

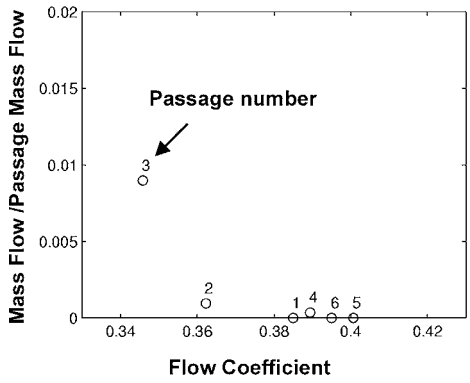

(*b*) **Leading edge spillage of tip clearance fluid below the blade tip**

Fig. 16 Tip clearance flow behavior in each blade passage at time (4): (*a*) spanwise distribution of pitch-averaged mass flow at passage exit plane and (*b*) leading-edge spillage of tip clearance fluid below the blade tip

The hypothesis presented concerning spike formation has practical implications for stall delay. Any technique that delays either of the two criteria that set the flow solution limit should result in a favorable movement of the stall point. Thus, both trailing-edge suction of the tip clearance backflow and leading-edge blowing, which would tend to delay the movement of the incoming/tip clearance flow interface to the leading-edge plane, should be effective in delaying the formation of spike disturbances and, thus, spike stall inception. One such example (although this is not the only explanation that can be given) is the observation by Lee and Greitzer [22] concerning the effect of end-wall suction and blowing on compressor stability. They reported that rear end-wall suction and/or leading-edge blowing were both effective in increasing the stall margin. Other examples (again with the above caveat) are the studies by Deppe et al. [21] and by Weigl et al. [23], which demonstrate the effectiveness of tip radially localized leading-edge blowing in delaying stall inception.

Summary and Conclusions

1. Net upstream (pitch- and time-averaged) mass flow at the trailing-edge blade tip, and (time-averaged) leading-edge tip

clearance flow spillage below the blade tip, are proposed as the two criteria that set the lowest flow coefficient at which a rotor blade passage can operate without the formation of spike disturbances.
2. These proposed criteria for the formation of spike disturbances are consistent with all published observations on axial compressor stall inception.
3. For compressors that exhibit short length-scale stall inception, techniques that delay either of the two proposed criteria for spike formation should be successful in extending the stable mass flow operating range.
4. The present work suggests that single blade passage computations may be used to predict stall inception if they contain:
   - exit flow boundary conditions that capture steady-state solutions past the peak pressure rise of a rotor blade (see the Appendix)
   - time-accurate computations so that the time-averaged flow field from oscillatory equilibrium solutions can be applied in the criteria for spike formation (Steady-state computations may not be suitable for cases with substantial unsteadiness from tip clearance flow oscillations, e.g., the large tip clearance case in Fig. 12, or interaction with adjacent blade rows.)
5. Based on the criteria presented, a conceptual framework that makes use of single blade passage computations for stall prediction in a compressor design system may be proposed:
   - Carry out single blade passage computations until the flow solution limit for all the blade rows in the compressor.
   - Find the flow solution limit with the highest mass flow and assess whether it occurs at a lower mass flow than the zero-slope peak of the (multistage) *compressor* stagnation-to-static pressure rise characteristic.
   - If yes, modal stall inception is predicted. If not, a spike disturbance is expected in the blade row that has its flow solution limit at the highest mass flow. The numerical approach by Gong et al. [5] then allows determination of whether the spike will grow to a fully developed rotating stall at this mass flow.

Acknowledgment

This work was funded by the U.S. Air Force Office of Scientific Research under Grant No. F49620-00-1-0014 monitored by Dr. T. J. Beutner, whose support is gratefully acknowledged. We would like to thank Prof. J. D. Denton and Dr. L. Xu for their help with setting up the code and computational mesh. The authors are also pleased to acknowledge Dr. J. J. Adamczyk, J. Bleeg, Dr. C. Hah, Dr. M. D. Hathaway, Dr. C. M. Rhie, Dr. H. Saathoff, and Dr. D. E. Van Zante, for providing useful information on features of the flow in other compressor geometries. Technical advice and insightful comments during the course of this work from Prof. E. E. Covert, Prof. N. A. Cumpsty, Dr. I. J. Day, Prof. J. J. Deyst, Dr. Y. Gong, Dr. T. P. Hynes, Prof. F. E. Marble, and Dr. J. P. Longley are also much appreciated. Finally, we would especially like to thank Dr. A. J. Strazisar for his thoughtful comments on the initial submission; the final version is better because of his input.

Appendix

UNSTREST [13] was used for time-accurate single and multiple blade passage computations. The mesh used for one passage was $106 \times 41 \times 45$ with a pinched blade tip and a tip clearance described by five radial grid points [6], which is standard for UNSTREST. As tip clearance flow is essentially a pressure-driven flow [8], the dominant effect of the pointed tip is to set an effective tip clearance size, rather than to alter the central features of the flow.

Because the same mesh is used for both the single and multiple (six) blade pitch computations, the upstream and downstream ducts are six blade pitches long. The length of the upstream and downstream ducts is set the same as the width of the multiple blade computational domain so that pressure disturbances with a wavelength equal to the domain width can decay to uniform conditions in the pitchwise direction at the boundaries. Consequently, the domain exit is far from the backflow region at the rotor trailing edge, thus avoiding reverse flow at the exit boundary.

The inlet boundary conditions consist of uniform stagnation pressure and temperature and axisymmetric radial distribution of swirl angle based on the spanwise distribution of the inlet guide vane exit angle in the E^3 compressor. A standard exit boundary condition, consisting of a specified axisymmetric tip static pressure with radial equilibrium, was implemented.

For single blade passage computations, the pressure rise versus flow curve in Fig. 4, points 1–4, was obtained by increasing the exit tip pressure until the flow solution limit (point 4) in increments of 0.005% of the dynamic pressure based on wheel speed. (For cases where the flow solution limit occurs at a flow coefficient lower than that of the peak exit static pressure—positively sloped part of the stagnation-to-static pressure-rise characteristic—a mass flow—throttle—exit boundary condition would be required. To initiate the stall flow transient (flow coefficients below point 4), the equilibrium flow limit is used as the initial solution, the back pressure is increased slightly, in this case by roughly 0.1% of the dynamic head based on blade tip speed.

For the multiple blade stall simulation, the single blade passage mesh and solution at the flow solution limit (point 4) are repeated six times pitchwise to provide the initial multiple blade flow solution limit. Circumferentially uniform inlet and exit conditions combined with the cylindrical coordinate system used in UNSTREST cause all the blade passages to stall simultaneously with the same transient.

Thus, a nonprejudicial (in terms of spike formation) inlet flow asymmetry was introduced through a full-span inlet stagnation pressure perturbation of six pitches in circumferential wavelength. The disturbance was applied only during ten blade passing times (about 1/20 of the development time of a spike). The total pressure inlet disturbance amplitude gave a rotor inlet velocity asymmetry of $\sim 1\%$ of rotor tip speed; this was viewed as representative of asymmetries encountered in practice.

References

[1] Moore, F. K., and Greitzer, E. M., 1986, "A Theory of Post-Stall Transients in Axial Compressors—Part I: Development of Equations," ASME J. Eng. Gas Turbines Power, **108**, pp. 68–76.
[2] Longley, J., 1994, "A Review of Non-Steady Flow Models for Compressor Stability," ASME J. Turbomach., **117**, pp. 202–215.
[3] Camp, T. R., and Day, I. J., 1998, "A Study of Spike and Modal Stall Phenomena in a Low-Speed Axial Compressor," ASME J. Turbomach., **120**, pp. 393–401.
[4] Day, I. J., 1993, "Stall Inception in Axial Flow Compressors," ASME J. Turbomach., **115**, pp. 1–9.
[5] Gong, Y., Tan, C. S., Gordon, K. A., and Greitzer, E. M., 1999, "A Computational Model for Short Wavelength Stall Inception and Development in Multistage Compressors," ASME J. Turbomach., **121**, pp. 726–734.
[6] Vo, H. D., 2001, "Role of Tip Clearance Flow on Axial Compressor Stability," Ph.D. thesis, Massachusetts Institute of Technology, Cambridge, MA.
[7] Khalid, S. A., Khalsa, A. S., Waitz, I. A., Tan, C. S., Greitzer, E. M., Cumpsty, N. A., Adamczyk, J. J., and Marble, F. E., 1999, "Endwall Blockage in Axial Compressors," ASME J. Turbomach., **121**, pp. 499–509.
[8] Storer, J. A., and Cumpsty, N. A., 1991, "Tip Leakage Flow in Axial Compressors," ASME J. Turbomach., **113**, pp. 252–259.
[9] Koch, C. C., 1974, "Discussion of Benser W. A.: Transonic Compressor Technology Advancements," Fluid Mechanics, Acoustics, and Design of Turbomachinery, Part II, NASA SP-304.
[10] Saathoff, H., and Stark, U., 2000, "Tip Clearance Flow Induced Endwall Boundary Layer Separation in a Single-Stage Axial-Flow Low-Speed Compressor," ASME Paper No. 2000-GT-0501.
[11] Silkowski, P. D., 1995, "Measurements of Rotor Stalling in a Matched and Mismatched Multistage Compressor," GTL Report No. 221, Massachusetts Institute of Technology, Cambridge, MA.
[12] Spakovszky, Z. S., Weigl, H. J., Paduano, J. D., Van Schalkwyk, C. M., Suder, K. L., and Bright, M. M., 1999, "Rotating Stall Control in a High-Speed Stage

With Inlet Distortion—Part I: Radial Distortion," ASME J. Turbomach., **121**, pp. 510–516.
[13] Denton, J. D., 1986, "The Use of a Distributed Body Force to Simulate Viscous Effects in 3D Flow Calculations," ASME Paper No. 86-GT-144.
[14] Cumpsty, N. A., 1996, private communication.
[15] Mailach, R., Lehmann, I., and Vogeler, K., 2000, "Rotating Instabilities in an Axial Compressor Originating From the Fluctuating Blade Tip Vortex," ASME Paper No. 2000-GT-506.
[16] Marz, J., Hah, C., and Neise, W., 2001, "An Experimental and Numerical Investigation Into the Mechanisms of Rotating Instability," ASME Paper No. 2001-GT-536.
[17] Hah, C., Schulze, R., Wagner, S., and Hennecke, D. K., 1999, "Numerical and Experimental Study for Short Wavelength Stall Inception in a Low-Speed Axial Compressor," AIAA Paper No. 99-IS-033.
[18] Day, I. J., and Freeman, C., 1994, "The Unstable Behavior of Low and High Speed Compressors," ASME J. Turbomach., **116**, pp. 194–201.
[19] Dobat, A., Saathoff, H., and Wulff, D., 2001, "Experimentelle Untersuchungen zur Entstehung von Rotating Stall in Axialventilatoren," VDI-Ber., **1591**, pp. 345–360.
[20] Park, H. G., 1994, "Unsteady Disturbance Structures in Axial Flow Compressor Stall Inception," M.S. thesis, Massachusetts Institute of Technology, Cambridge, MA.
[21] Deppe, A., Saathoff, H., and Stark, U., 2005, "Spike-Type Stall Inception in Axial-Flow Compressors," *6th European Conference on Turbomachinery—Fluid Dynamics and Thermodynamics*, Lille, France, March, pp. 178–188.
[22] Lee, N. K. W., and Greitzer, E. M., 1990, "Effects of Endwall Suction and Blowing on Axial Compressor Stability Enhancement," ASME J. Turbomach., **112**, pp. 133–144.
[23] Weigl, H. J., Paduano, J. D., Frechette, L. G., Epstein, A. H., Greitzer, E. M., Bright, M. M., and Strazisar, A. J., 1998, "Active Stabilization of Rotating Stall and Surge in a Transonic Single Stage Compressor," ASME J. Turbomach., **120**, pp. 625–636.